Proceedings of the 28th IEEE
EMBS Annual International Conference
New York City, USA, Aug 30-Sept 3, 2006

Multilevel Homogenization Applied to the Cardiac Bidomain Equations

Travis Austin, Mark Trew, and Andrew Pullan

Abstract— **Accurate cardiac tissue-based modeling using the bidomain equations requires the incorporation of fine-scale structures observed at the 50-100 micron level. By including such features we can more easily observe how defibrillation shocks lead to total depolarization of the heart. Several modeling studies that have investigated the effect of fine scale structures on defibrillation success have been completed. Results have shown that such structures aid, through the creation of virtual electrodes, in total depolarization. An obstacle that occurs with this modeling style is the massive amount of data that must be incorporated into detailed tissue models for even a cubic millimeter sample of cardiac tissue. In this paper, we discuss our approach to generating upscaled, or homogenized, versions of these models that can be used to perform simulations at a more reasonable modeling scale. They have the advantage of incorporating fine scale structure into the model at a reduced modeling cost. We introduce and briefly explore the advantages of this upscaling method.**

I. INTRODUCTION

THE ability to perform computer simulations of electrical propagation in cardiac tissue is beginning to yield insights previously unrealised with experimental studies alone [1], [2]. Our group at the University of Auckland has provided several insightful studies using the discontinuous bidomain equations that account for structural information obtained from tissue segmentation of rat and pig cardiac tissue samples [3], [4].

A burden of this work is attempting to reasonably incorporate the massive amount of data generated in the imaging process into the numerical model. Since it is infeasible to incorporate all of the data into the model, a means of capturing the coarse scale features of the data within the numerical model is vital.

Ad hoc homogenization approaches based on simple averaging have been used in the past to generate coarse representations of the fine scale data. In this paper, we introduce a new method, based on multilevel upscaling [5], that allows us to build a homogenized model using a sound mathematical approach. We do not explicitly generate coarse scale representations of the data, but instead coarse scale representations of the matrices generated by the fine scale data.

The key step in the homogenization process uses a matrix triple product that is often used to build coarse grid matrices in multigrid. This triple product is defined by an interpolation operator, and furthermore, the choice of interpolation operator significantly influences the properties of the coarse grid matrix. For interpolation, we either use one that preserves certain properties of the flux or one that is linear. Which interpolation is employed depends upon the properties of the matrix that we are homogenizing.

The package that provides the homogenization tools, called JedPack, is a F95 code built on top of the Black Box Multigrid solver [6]. With JedPack we can easily run homogenized cardiac bidomain simulations, and be guaranteed of fast simulations because of the ability to make use of the robust Black Box Multigrid solver. In the remainder, we describe our approach and show preliminary computational results.

Authors are with the Bioengineering Institute, University of Auckland, Auckland, New Zealand. Email: t.austin@auckland.ac.nz

II. METHODS

A. Cardiac Bidomain Equations

The cardiac bidomain equations consist of a nonlinear reaction-diffusion equation coupled to an elliptic equation. Together these equations describe the flow of electrical current between the intracellular and extracellular spaces of cardiac tissue [7].

To express these equations mathematically, we introduce the extracellular potential ϕ_e and the transmembrane potential $V_m = \phi_i - \phi_e$, where ϕ_i is the intracellular potential. Let the intracellular and extracellular spaces have conductivities denoted by $\boldsymbol{\sigma}_i$ and $\boldsymbol{\sigma}_e$, and express the corresponding diffusion operators as $\mathcal{L}_i[\,\cdot\,] = -\nabla\cdot(\boldsymbol{\sigma}_i\nabla[\,\cdot\,])$ and $\mathcal{L}_e[\,\cdot\,] = -\nabla\cdot(\boldsymbol{\sigma}_e\nabla[\,\cdot\,])$. The bidomain equations are then

$$A_m C_m \frac{\partial V_m}{\partial t} + \mathcal{L}_i V_m = -\mathcal{L}_i \phi_e - A_m I_{ion}(V_m) \quad (1)$$

$$(\mathcal{L}_i + \mathcal{L}_e)\phi_e = -\mathcal{L}_i V_m + i_e(t), \quad (2)$$

where A_m is the surface-to-volume ratio of the cell membrane, C_m is the membrane capacitance per unit area, and i_e is extracellular current injection. We use a simple cubic cell model for this study, such that

$$I_{ion}(V_m) = g\left[V_m\left(1-\frac{V_m}{V_{th}}\right)\left(1-\frac{V_m}{V_p}\right)\right], \quad (3)$$

where g is membrance conductance, V_{th} and V_p are the threshold and plateau potentials, and all potentials are deviations from resting potential, V_r [7].

We apply standard boundary conditions in this work so that

$$(\boldsymbol{\sigma}_i\nabla V_m)\cdot\mathbf{n} = -(\boldsymbol{\sigma}_i\nabla\phi_e)\cdot\mathbf{n} \quad (4)$$

are the boundary conditions on V_m and

$$(\boldsymbol{\sigma}_e\nabla\phi_e)\cdot\mathbf{n} = 0 \quad (5)$$

are the boundary conditions on ϕ_e. While Dirichlet conditions are often used on ϕ_e, e. g. for applying shocks, we restrict ourselves in this work to no flux boundary conditions.

We use a semi-implicit split-step strategy for time integration [8], which utilizes a first-order forward time step to approximate $\partial V_m/\partial t$. The spatial domain is a cuboid, and our finite element discretization uses tensor-product trilinear finite elements. The following algorithm describes the approach taken to updating V_m and ϕ_e at each time step. Note $\mathbf{v}$ and $\mathbf{p}$ denote discrete versions of V_m and ϕ_e.

1. Calculate $\mathbf{I}_{ion}^{t+\Delta t/2}$ from $\mathbf{v}^t$ via (3).
2. Given $\mathbf{v}^t$, ϕ^t, and $\mathbf{I}_{ion}^{t+\Delta t/2}$ solve

$$(C_m\overline{\mathbf{M}} + \Delta t\,\mathbf{A}_i)\,\mathbf{v}^{t+\Delta t} = C_m\overline{\mathbf{M}}\,\mathbf{v}^t - \Delta t\,\mathbf{A}_i\mathbf{p}^t - \mathbf{M}\,\mathbf{I}_{ion}^{t+\Delta t/2} \quad (6)$$

   for $\mathbf{v}^{t+\Delta t}$.
3. Given $\mathbf{v}^{t+\Delta t}$ and source $\mathbf{I}_e^{t+\Delta t}$ solve

$$(\mathbf{A}_i + \mathbf{A}_e)\mathbf{p}^{t+\Delta t} = -\mathbf{A}_i\mathbf{v}^{t+\Delta t} + \mathbf{M}\,\mathbf{I}_e^{t+\Delta t} \quad (7)$$

   for $\mathbf{p}_e^{t+\Delta t}$.

Furthermore, in (6), the matrix $\overline{\mathbf{M}}$ is defined by

$$\left(\overline{\mathbf{M}}\mathbf{v}, \mathbf{v}\right)_0 = \int_\Omega A_m V_m V_m \,\mathrm{d}\Omega. \quad (8)$$

In (6) and (7), $\mathbf{M}$ is a mass matrix and $\mathbf{A}_i$ and $\mathbf{A}_e$ are matrices representing the continuous operators $\mathcal{L}_i$ and $\mathcal{L}_e$.

B. Tissue Features

In most studies of electrical activation in cardiac tissue, the parameters describing the physics are continuous. There are two possible reasons for this. First, in the cardiac electrophysiology community, the dominant view of tissue structure is that of syncytial cell-to-cell networks at the microscale and a smoothly varying fiber field at higher scales. These structural features are homogenized into the effective conductivity tensors of the bidomain equations. However, there is an emerging number of cardiac imaging, histological and even electrical recording studies that show evidence of mezoscale tissue structures, such as interlaminae clefts or cleavage planes, imposing rapidly varying or discontinuous electrical behavior.

The second driver for continuous tissue property modeling studies has been the use of numerical techniques, such as finite difference methods [8], that discretize the strong form of the bidomain equations. These techniques rely on assumptions regarding the differentiability of the conductivity tensors and, hence, tissue properties must be smoothly varying and continuous. Methods based on discretizing the weak forms of the bidomain equations, such as finite element [9] or finite volume methods [10] relax this requirement of smoothly varying properties and enable the study of discontinuous properties.

Detailed tissue imaging (see Figure 1) [11] together with measurements [4] and tissue-specific modeling studies [3] have shown that mezoscale tissue structures can significantly impact the spread of electrical activation in cardiac tissue. However, the explicit inclusion of these structures rapidly results in intractable computer models. Thus, we present an innovative approach that enables the expression of high resolution tissue structural features in lower resolution computer models. This multilevel homogenization method is based on Black Box Multigrid.

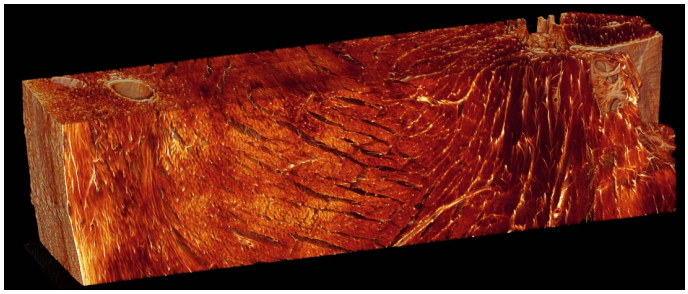

Fig. 1. Extended confocal image of transmural segment of rat ventricular myocardium. The image spans from the the epicardium (left) to the endocardium (right).

C. Multilevel Homogenization with Black Box Multigrid

Black Box Multigrid (BoxMG) is one of several variants of multigrid. It is defined by a hierarchy of grids on which error components of different frequencies can be eliminated [6]. The difference between BoxMG and traditional multigrid is that BoxMG maintains optimal convergence for discontinuous problems by its judicious choice of interpolation operator [9].

The hierarchy of grids employed by BoxMG is accompanied by a hierarchy of matrices. At each level of the hierarchy, the matrix approximates the original fine grid matrix on that level. In [12] the authors considered BoxMG as a tool for obtaining homogenized diffusion coefficients. More recently, in [5], BoxMG was used to obtain a fine grid solution at a reduced cost by mainly performing work on the coarse grid.

The algorithm described in [5] focused on the steady state diffusion equation of porous media flow. Our preliminary investigations showed it was inappropriate to use their approach for the time-dependent bidomain equations. So we have introduced the multilevel upscaling concept of [5] into the bidomain equations in a way that we feel is appropriate for time-dependent problems.

In our approach, BoxMG is used to generate coarse grid versions of certain fine grid matrices. The coarse grid matrices are obtained when building the multigrid hierarchy that accompanies solving a system using BoxMG. For example, if $\mathbf{A}^h$ is the matrix on grid level h, then the coarse matrix is defined by the triple product

$$\mathbf{A}^H := \mathbf{P}_H^T\mathbf{A}^h\,\mathbf{P}_H, \quad (9)$$

where $\mathbf{P}_H$ is the interpolation operator from grid level H to grid level h. These coarse grid matrices are stored and used in future simulations taking place at the resolution associated with grid level H. In contrast to [5], where the fine grid matrix was retained for post-processing needs, we run simulations solely using the coarse grid matrices, and perform no post-processing.

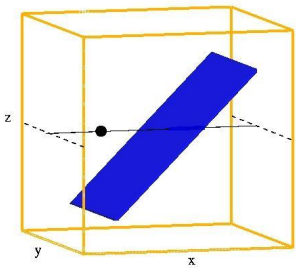

Fig. 2. An illustration of the artificial cleavage plane (blue plane) and the extracellular stimulus cite (black dot) for Problem A. Also the dashed line intersecting the artificial cleavage plane describes where we plot the solution for Figure 3.

The triple product (9) is not used to homogenize each and every matrix in (6) and (7). Instead only those matrices that are generated from discontinuous data and need homogenization. Here, discontinuous data is used to build the mass matrix, $\overline{\mathbf{M}}$, and the diffusion equation, $\mathbf{A}_i$. For these two matrices, we call setup of the Black Box Multigrid solver, which generates the coarse grid matrices at each level per (9), and in a file, we store the coarse grid matrix at the level desired. Note that we are not merely building coarse grids, which is trivial, but constructing coarse scale representations of fine scale operators, which is not trivial.

Lastly the proper $\mathbf{P}_H$ to be used in (9) depends on the kind of matrix. For a mass matrix, like the one defined by (8), linear interpolation used in (9) yields a coarse grid matrix which is representative of a mass matrix with an averaged value of the coefficient [13]. For a diffusion matrix, there is no averaging of the diffusion coefficient that yields an accurate homogenized operator [14]. That is why the BoxMG interpolation operator is used for the diffusion matrix since it preserves flux conservation, and yields a coarse grid matrix that accurately approximates the coarse scale behavior of the fine grid matrix [13].

D. Model Problems

We present computational results for two test problems, denoted Problem A and B. Problem A is used to establish the validity of the method. Hence the domain of the problem is the unit cube with a volume of $1.0\ \mathrm{mm}^3$. See Figure 2. As illustrated in this figure, we place a single plane within the tissue sample that represents a plane of tissue that is non-conducting in intracellular space. It is a simple, artificial example that is representative of the kind of discontinuous plane that we encounter in our modeling studies.

The finest mesh has a resolution of $1/128\ \mathrm{mm}$ in each direction, and on this mesh, the artificial cleavage plane is $3/128\ \mathrm{mm}$ thick. We perform simulations on coarser meshes with resolutions of $1/64\ \mathrm{mm}$ and $1/32\ \mathrm{mm}$. The time step is $0.01\ \mathrm{ms}$ and the duration of the simulations was $10\ \mathrm{ms}$. Boundary conditions for V_m and ϕ_e are both no flux conditions. A constant conductivity value of $0.375\ \mathrm{mS/mm}$ is used in intracellular and extracellular space. The surface-to-volume ratio is $300.0\ \mathrm{mm}^{-1}$ and the membrane capacitance is $0.01\ \mu F/\mathrm{mm}^2$. A $10000\ \mathrm{mA/mm}^3$ unipolar source, centered at $(0.25\ \mathrm{mm}, 0.5\ \mathrm{mm}, 0.5\ \mathrm{mm})$, is applied at $0.1\ \mathrm{ms}$ for $4.9\ \mathrm{ms}$.

Space	Fiber	Sheet	Sheet-Normal
Intracellular	0.25	0.125	0.125
Extracellular	0.2	0.0416	0.0416

TABLE I

INTRACELLULAR AND EXTRACELLULAR VALUES USED FOR TEST PROBLEM 2 WITH DATA COMING FROM CARDIAC TISSUE TAKEN FROM A RAT.

Problem B comes from cardiac tissue drawn from a rat heart. The image found in Figure 1 was reconstructed from the data obtained by segmentation. The size of the tissue is $3.84 \times 1.12 \times 0.96\ \mathrm{mm}^3$. Cleavage planes and vasculature are found throughout the tissue producing a mesh where 16% of the elements are associated with intracellular void space. As mentioned previously, this affects intracellular conductivity, $\boldsymbol{\sigma}_i$, and the surface-to-volume ratio, A_m.

The finest mesh used for the second test problem has a resolution of $1/100\ \mathrm{mm}$. Simulations are performed on a coarser grid having a resolution of $1/25\ \mathrm{mm}$. The time step is $0.01\ \mathrm{ms}$ and simulations are performed for $10\ \mathrm{ms}$. Anisotropy is allowed and the the fiber, sheet, and sheet-normal conductivity values are as in Table I. Fiber orientation is set to be in the x-direction for simplicity. The surface-to-volume ratio is $300.0\ \mathrm{mm}^{-1}$ and the membrane capacitance is $0.01\ \mu\mathrm{F/mm}^2$. As a source, we use a cell stimulus with amplitude $1000\ \mu\mathrm{A/mm}^3$, and a duration of $5\ \mathrm{ms}$. The cell stimulus is initiated at $0.1\ \mathrm{ms}$.

III. RESULTS

A. Problem A

Results for Problem A are represented by the two illustrations in Figure 3. This figure shows V_m plotted along the dashed line (in the interior of the domain) from Figure 2 at $5\ \mathrm{ms}$. This is just as the stimulus is terminated but a propagation has already taken hold. On coarser grids the appropriate coarse grid versions of $\mathbf{A}_i$ and $\overline{\mathbf{M}}$ are used, which capture the coarse-scale influence of the cleavage plane. For illustration purposes we have also included the same problem ran without a cleavage plane. The line drawn through the domain intersects the artificial cleavage plane yielding a discontinuity in the solution gradient as illustrated by the two figures. Of particular significance is the solution seen in the second part of Figure 3, which shows that the various coarse grid simulations capture the coarse-scale behavior.

B. Problem B

Results for Problem B are represented by the three illustrations in Figure 4. We have plotted the transmembrane solution at $3\ \mathrm{ms}$ for a slice of the tissue. The slice represented

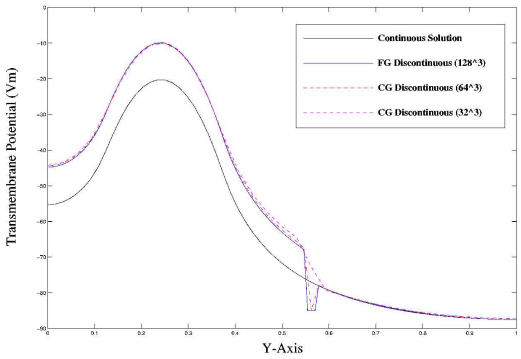

(a) Solution for $0 \leq y \leq 1$

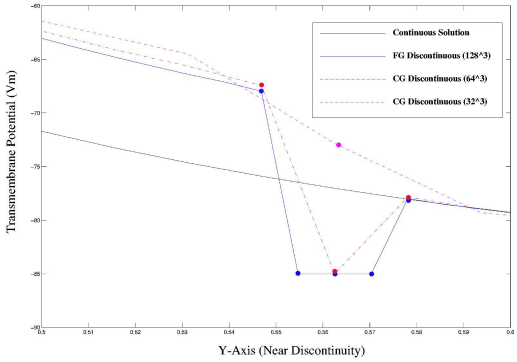

(b) Solution for $0.5 \leq y \leq 0.6$

Fig. 3. *Two illustrations of transmembrane solution at* $t = 5$ ms *for* $x = z = 0.5$ mm. *First illustration is for the entire* y*-domain and the second is focused on the region around the artificial cleavage plane. Together the illustrations show the ability of the homogenization approach to capture key coarse scale behavior.*

in the figure is for a fixed $y = 0.56$ mm. The three plots show (a) the solution for the original fine grid problem (b) the solution for the homogenized model and (c) the solution at the same coarse level for a continuous model. Appearances of the transmembrane potential in (b) show that our homogenization approach picks up key characteristics of the cleavage planes.

IV. Conclusion

In this paper we have presented ideas on using Black Box Multigrid for creating homogenized operators. Our results illustrate that the method shows great promise in that it clearly captures key behavior for simple model problems (Problem A), and is able to produce a solution with similar characteristics to the original fine grid problem for a realistic data set (Problem B). Future work must focus on providing a clear measure of how well our method represents the coarse scale behavior. We have investigated several of these methods in brief, but will report on these details at a future date.

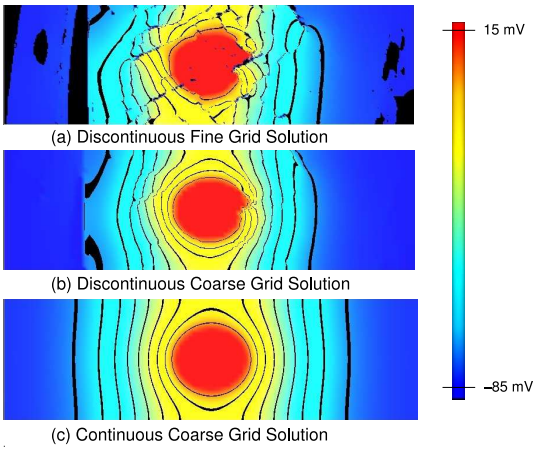

Fig. 4. *Transmembrane solution* (V_m) *at 3 ms in the* xz*-plane (at* $y = 0.56$ mm*). Stimulus is located in the center of the domain (a sphere with radius* 0.2 mm*) and has a duration of* 5 ms*. Coarse grid discontinuous solution was obtained using homogenization of appropriate fine grid operators, and captures some of the key variation in* V_m*. Continuous solution is added as a reference.*

References

[1] I. R. Efimov, F. Aguel, Y. Cheng, B. Wollenzier, and N. Trayanova, "Virtual electrode polarization in the far field: implications for external defibrillation," *Am J Physiol Heart Circ Physiol*, vol. 279, no. 3, pp. H1055–1070, 2000.

[2] B. J. Roth and S. G. Patel, "Effects of elevated extracellular potassium ion concentration on anodal excitation of cardiac tissue," *J. Cardiovasc. Electrophysiol.*, vol. 14, no. 12, pp. 1351–1355, 2003.

[3] D. A. Hooks, M. L. Trew, B. H. Smaill, and A. J. Pullan, "Do intramural virtual electrodes facilitate successful defibrillation? model based analysis of experimental evidence," *J. Cardiovasc. Electr.*, vol. 17, no. 3, pp. 305–311, 2006.

[4] M. L. Trew, B. J. Caldwell, G. B. Sands, D. A. Hooks, D. C.-S. Tai, T. M. Austin, I. J. LeGrice, A. J. Pullan, and B. H. Smaill, "Cardiac electrophysiology and tissue structure: Bridging the scale gap with a joint measurement and modelling paradigm," *Experimental Physiology*, vol. 91, no. 2, pp. 355–370, 2006.

[5] S. MacLachlan and J. Moulton, "Multilevel upscaling through variational coarsening," *Water Resour. Res.*, vol. 42, no. 2, 2006.

[6] J. Dendy Jr., "Black box multigrid," *J. of Comp. Phys.*, vol. 48, pp. 366–386, 1982.

[7] A. Pullan, M. Buist, and L. Cheng, *Mathematically Modelling the Electrical Activity of the Heart*. Singapore: World Scientific Publishing Company, 2005.

[8] M. Buist, G. Sands, P. Hunter, and A. Pullan, "A deformable finite element derived finite difference method for cardiac activation problems," *Annals of Bio-Med Eng.*, vol. 31, pp. 577–588, 2003.

[9] T. M. Austin, M. L. Trew, and A. J. Pullan, "Solving the cardiac bidomain equations for discontinuous conductivities," *IEEE in Biomed. Eng.*, vol. 53, no. 7, pp. 1265–1272, 2006.

[10] M. L. Trew, I. J. LeGrice, B. H. Smaill, and A. J. Pullan, "A finite volume method for modeling discontinuous electrical activation in cardiac tissue," *Annals of Bio-Med Eng.*, vol. 33, no. 5, 2005.

[11] G. B. Sands, D. A. Gerneke, D. A. Hooks, C. R. Green, B. H. Smaill, and I. J. LeGrice, "Automated imaging of extended tissue volumes using confocal microscopy," *Microsc. Res. Tech*, vol. 67, pp. 227–239, 2005.

[12] J. Moulton, J. Dendy Jr., and J. Hyman, "The black box multigrid numerical homogenization algorithm," *J. of Comp. Phys.*, vol. 142, pp. 80–108, 1998.

[13] S. Knapek, "Matrix-dependent multigrid homogenization for diffusion problems," *SIAM J. Sci. Computing*, vol. 20, no. 2, pp. 515—533, 1998.

[14] X.-H. Wen and J. Gomez-Hernandez, "Upscaling hydraulic conductivities in heterogeneous media: An overview," *J. of Hydrology*, vol. 183, pp. ix–xxii, 1996.